Journal of Theoretical Biology 453 (2018) 1–13

Contents lists available at ScienceDirect

Journal of Theoretical Biology

journal homepage: www.elsevier.com/locate/jtbi

Epidemics on plants: Modeling long-range dispersal on spatially embedded networks

Juddy H. Arias[a], Jesus Gómez-Gardeñes[b,c], Sandro Meloni[d,e], Ernesto Estrada[f,*]

[a] Department of Mathematics, Universidad del Valle, Colombia
[b] GOTHAM Lab, Institute for Biocomputation and Physics of Complex Systems (BIFI), University of Zaragoza, Zaragoza, Spain
[c] Department of Condensed Matter Physics, University of Zaragoza, Zaragoza, Spain
[d] Institute for Biocomputation and Physics of Complex Systems (BIFI), University of Zaragoza, Zaragoza 50018, Spain
[e] Department of Theoretical Physics, University of Zaragoza, Zaragoza 50009, Spain
[f] Department of Mathematics & Statistics, University of Strathclyde, 26 Richmond Street, Glasgow, G11XH, UK

ARTICLE INFO

Article history:
Received 23 January 2018
Revised 3 May 2018
Accepted 4 May 2018
Available online 5 May 2018

Keywords:
Plant diseases
Spatial networks
Susceptible-Infected- Susceptible
Susceptible-Infected-Recovered

ABSTRACT

Here we develop an epidemic model that accounts for long-range dispersal of pathogens between plants. This model generalizes the classical compartmental models–Susceptible-Infected-Susceptible (SIS) and Susceptible-Infected-Recovered (SIR)–to take into account those factors that are key to understand epidemics in real plant populations. These ingredients are the spatial characteristics of the plots and fields in which plants are embedded and the effect of long-range dispersal of pathogens. The spatial characteristics are included through the use of random rectangular graphs which allow to consider the effects of the elongation of plots and fields, while the long-range dispersal is implemented by considering transformations, such as the Mellin and Laplace transforms, of a generalization of the adjacency matrix of the geometric graph. Our results point out that long-range dispersal favors the propagation of pathogens while the elongation of plant plots increases the epidemic threshold and decreases dramatically the number of affected plants. Interestingly, our model is able of reproducing the existence of patchy regions of infected plants and the absence of a clear propagation front centered in the initial infected plants, as it is observed in real plant epidemics.

1. Introduction

Understanding the spread of pathogens on plants has always been an important challenge for agricultural and environmental development (Campbell and Madden, 1990; Segarra et al., 2001). Today, it is well-documented that the long-range dispersal of pathogenic fungi is responsible for the spread of several important crop diseases at distances ranging from a few meters to thousands of kilometers (Brown and Hovmø ller, 2002). Many of these fungi, such as those causing diseases like rust, powdery mildew, and downy mildew diseases, produce a massive numbers of spores which are then dispersed by wind from one plant to another. Such kind of wind dispersal is an important surviving mechanism for the spores, which can travel even at inter-continental distances (Brown and Hovmø ller, 2002). Another mechanism of long-range dispersal of pathogenic organisms is by means of vectors (Gillespie et al., 2012), ranged from small insets to humans, which transport the inoculum of the pathogen from one plant to another. Both mechanisms are believed to be responsible for the dispersal of diseases such as Dutch elm disease (Swinton and Gilligan, 1996), citrus canker (Gottwald et al., 2001), sudden oak death (Rizzo et al., 2002) and rhizomania of sugar beet (Stacey et al., 2004). The study of long-range dispersal in plants is not only of remarkable importance for understanding plant diseases but also for other plant-related processes (Clark, 1998; Clark et al., 1999; Levin et al., 2003; Nathan, 2006). For instance, most of the transport of pollen between plants is carried out by wind or insect pollinators. This biological process is vital for the survival of the species, but it is also important for understanding transgenic pollen dispersal (Vallaeys et al., 2017). Of similar importance is the spreading of evolutionary novelties across populations. Recently, it has been recognized that rare-events of long-range jumps can lead to drastic acceleration of these processes (Hallatschek and Fisher, 2014).

In order to model epidemic processes in plants the modeler dispose of several theoretical tools (Jeger, 1990; Kranz, 2012; Moslonka-Lefebvre et al., 2011; Van Maanen and Xu, 2003), not without a few important challenges (Cunniffe et al., 2016, 2015; Riley et al., 2015). The incorporation of long-range dispersal effects,

* Corresponding author.
E-mail address: ernesto.estrada@strath.ac.uk (E. Estrada).

https://doi.org/10.1016/j.jtbi.2018.05.004
0022-5193/

either as diffusive processes or by including long-range jumps, has been the topic of many researches (Allen and Ernest, 2002; Aylor, 2003; Davis, 1987; Dybiec et al., 2009; Filipe and Maule, 2004; Keeling et al., 2001; Kleczkowski and Grenfell, 1999; Kot et al., 1996). Recently, Vallaeys et al. (2017) have stressed that the diffusive process "*often seriously underestimates dispersal distances*", and on the other hand, pure Lévy movements "*often overestimates dispersal distances*". Thus, methods that account for an equilibrated balance between diffusive and long-range dispersal are still needed for modeling epidemic processes in plants (Vallaeys et al., 2017). Another important challenge in modeling plant diseases is the necessity to consider the spatial characteristics of the plots or fields in which the plants are embedded. As a consequence, those models that consider spatial features for characterizing the structure of populations in heterogeneous landscapes have gained recent interest (Jeger et al., 2007). One approach is to consider spatial networks that treat interactions as a continuous variable that decays with increasing distance. Another, which is interesting from the perspective of the current work, is to distribute randomly and independently a set of points on the Euclidean plane to represent the relative spatial location of individual host plants or habitat patches (Jeger et al., 2007). The second kind of models give rise to *random geometric graphs* (RGGs) (Bollobás, 1985; Dall and Christensen, 2002; Gilbert, 1959; Penrose, 2003), in which each node is randomly assigned geometric coordinates and then two nodes are connected if the (Euclidean) distance between them is smaller than or equal to a certain threshold r. For instance, let us suppose that a pathogen located in a plant i can jump and infect any susceptible plant inside a certain radius centered on i. This implies that every other node inside the disk of radius r centered at the infected node i is connected to it.

In this work we are interested in epidemic processes similar to the transmission of viruses on plants, which are known to occur mainly transmitted by insect vectors of several families, with Hemiptera being by far the most important group (Fereres and Moreno, 2009). For instance, homopterans (a subclass formed by two suborders of Hemiptera) are vectors for about 55% of all known plant viruses, with aphids transmitting approximately 275 virus species (more than 50% of plant viruses vectored by insects) and whiteflies transmitting 114 virus species (Jones, 2003; Nault, 1997). Aphids represent a vast group of insects covering about 4700 species, from which 450 species are involved in colonizing food and fiber crop (see Fereres and Moreno (2009) and references therein). In this way of vectored transmission of diseases on plants a nontrivial aspect of the transmission are the behavioral events related to the vectors. These are a series of successive events followed by vectors that ends up in virus transmission on the plant. In the case of aphids, it has been recognized that the following events are important (Powell et al., 2006): (i) pre-alignment before landing, (ii) plant contact and assessment of surface cues after landing, (iii) probing on superficial tissues, (iv) location and insertion of styletes at the appropriate feeding site, (v) salivation followed by committed sap ingestion. From the point of view of modeling the epidemic spreading, the event of pre-alignment before landing is of vital importance. For instance, it is not true that an insect simply hop from one plant to another but in some occasions they can remain flying for long periods (2 h for whiteflies or 7 h for *N. virescens* females) until "attractive" plants are founds for landing. Then, some insects hop from a plant to a close one, e.g., *H. coagulata* which tends to make short flights of no more than 5 m, and others can travel longer distance during their long flying times. For an excellent review and discussion see ref. Fereres and Moreno (2009). It is also important to notice that although a plant can be selected for landing by an insect due to its attractiveness, it may or may not be potential host for that insect, and that the discrimination appears after landing and probing on different plants (Kring, 1972). All these factors makes the hopping process of insect vectors a nontrivial one and here we propose a way of capturing some of these nontrivialities into a model for epidemic spreading on plants.

The fact that plants are not mobile as humans and animals produces lower mixing levels in a given population. Consequently, the shape of the plot or field in which the plants are distributed affects significantly disease dynamics in these systems. In fact, there are both empirical and theoretical evidence that support this hypothesis (Bonnot et al., 2010; Ferrandino, 2005; Fleming et al., 1982; Mundt and Brophy, 1988; Mundt et al., 1996; Paysour and Fry, 1982; Waggoner, 1962; Xu and Ridout, 2000). In general, it has been suggested that square plots and fields favor higher spreading of plant diseases than elongated ones of the same area (Fleming et al., 1982; Paysour and Fry, 1982; Waggoner, 1962). It is important to remark that the area of the field also plays a fundamental role, with larger plots and fields favoring more the spreading of diseases (Ferrandino, 2005; Mundt et al., 1996; Xu and Ridout, 2000). Also, the orientation of elongated fields may affect the disease propagation with orientations perpendicular to prevalent winds suppressing epidemic progression (Fleming et al., 1982; Waggoner, 1962). All in all, for plots and fields of the same area and orientation there is empirical and theoretical evidence that elongated shapes decreases the impact of epidemics on plant populations. It is worth noting that the theoretical models (Ferrandino, 2005; Mundt and Brophy, 1988; Xu and Ridout, 2000) used in the previously mentioned studies do not use network theory as a tool for the study of epidemic spreading. Recently, Estrada et al. have generalized the RGGs to consider rectangular areas (Estrada and Chen, 2015; Estrada and Sheerin, 2015, 2016) and have used them as plant fields to show analytically and computationally that the rectangular elongation of these fields produces a significant delay on the disease propagation on plants (Estrada et al., 2016).

In this work we develop a new model that combines three desirable ingredients for modeling plant diseases: (i) a network environment in which the proximity between plants determines their connectivity, (ii) the spatial embeddedness of plants in areas of different shapes, (iii) inclusion of long-range jumps allowing distance-dependent dispersal of pathogens. The model is based on a generalization of classical epidemiological models, such as Susceptible-Infected-Susceptible (SIS) and Susceptible-Infected-Recovered (SIR) models, in which the infection is propagated through the nodes and edges of a spatial network and in which long-range dispersal of the disease is allowed. The spatial networks used here allow to study the effect of elongation of plant crops and fields on the dispersal of the pathogen. We first formulate mathematically this model and then use it for the analysis of epidemic spread on hypothetical plant plots. According to our current results the propagation of pathogens through plants when long-range dispersal is present is characterized by the following general patterns: (i) much faster propagation of disease than in normal diffusive regimes, (ii) the elongation of plant plots/fields increases the infectivity needed to trigger the epidemics; (iii) the elongation of the plots/fields decays dramatically the number of affected plants; (iv) the number of plants dead (removed) in a very elongated plot/field is much less when the dynamics is controlled by a Mellin transform than when it is controlled by a Laplace one; (v) the dynamics is characterized by the existence of patchy regions of infected plants and by the absence of a clear propagation front that separates infected from noninfected plants.

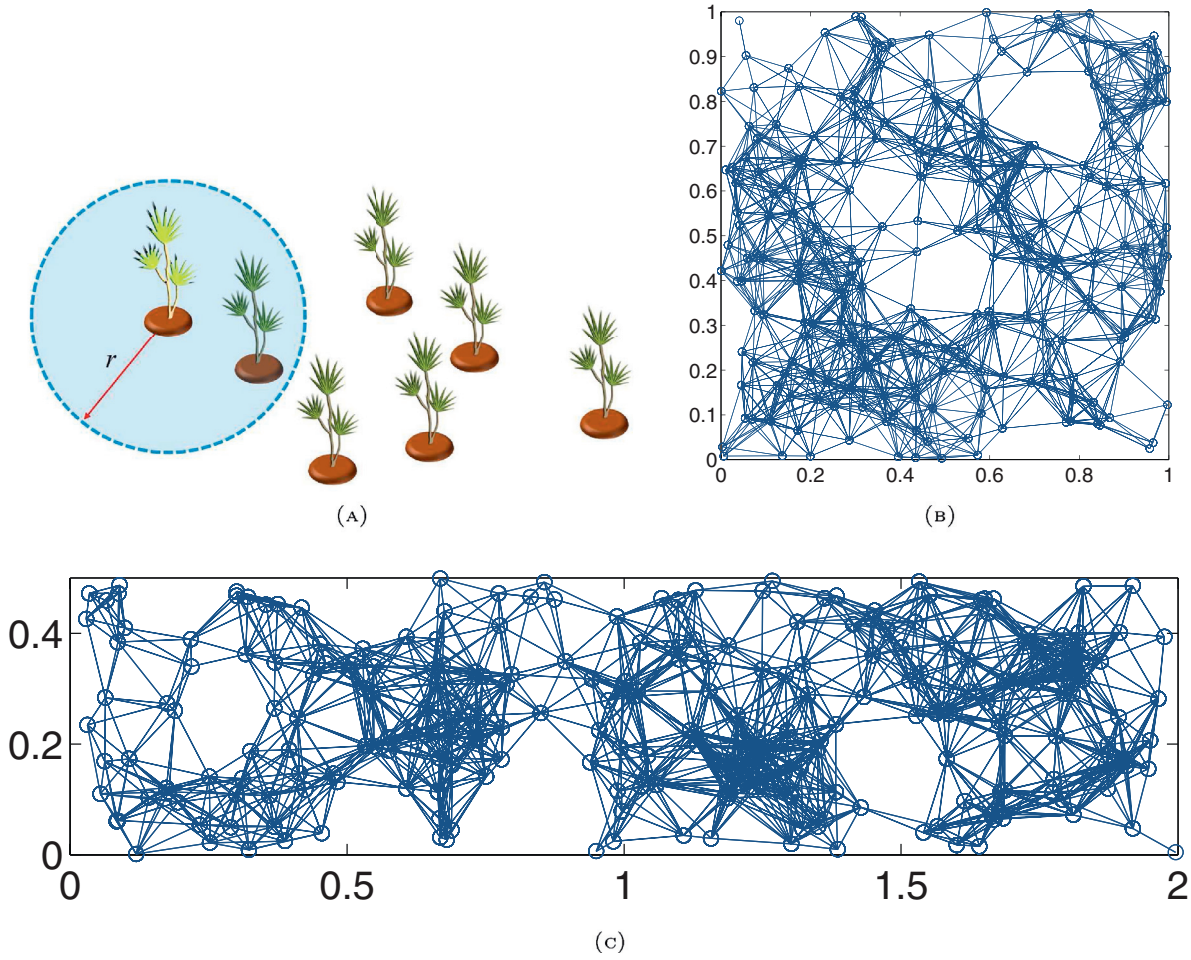

Fig. 1. Schematic illustration of a random distribution of plants in a plot or field (a), a squared random geometric graph (b) and an elongated random rectangular graph (c).

2. The model

2.1. Modeling scenario

Here we consider plants represented by the nodes of a graph $G = (V, E)$. The plants are assumed to be randomly and independently distributed (see Fig. 1(a)) on a given plot or field of rectangular shape and unit area. Then, we model such scenario by a random rectangular graph (RRG). An RRG is defined by considering a rectangle $[0, a] \times [0, b]$ where $a, b \in \mathbb{R}$, $a \geq b$. For the sake of simplicity we will consider unit rectangles of the form $[0, a] \times [0, a^{-1}]$. The construction of the RRG is as follow. We distribute randomly and independently n points on this rectangle. We then center at each point a disk of radius r, which hereafter we call the influence radius. In Fig. 1(a) we illustrate a possible connection radius for the plant in the center. It indicates that the pathogen can jump to any plant which is at a distance shorter or equal than r. Notice that for the construction of RRG only one radius for each node is used and it remains fixed for all the experiments. Let i be an arbitrary plant in the rectangle and let D_i be the disk of radius r centered at i. Then, we connect every node inside the disk D_i to the point i. By doing so for each of the n points we construct the RRG. When $a = 1$ the rectangle $[0, a] \times [0, a^{-1}]$ is simply the unit square $[0, 1]^2$. This model is known as the random geometric graph (RGG) and has been widely studied in the mathematical literature. In Fig. 1((b) and (c)) we illustrate two RRGs with different values of the rectangle side length a and the same number of nodes and edges. In Fig. 1(b) when $a = 1$ the graph corresponds to the classical random geometric graph in which the nodes are embedded into a unit square. The case illustrated in Fig. 1(c) corresponds to $a = 2$ and it represents a slightly elongated rectangle. The adjacency matrix of the RRG is defined as the matrix $A \in \mathbb{R}^{n \times n}$ whose entries are given by

$$A(i, j) = \begin{cases} 1 & if\ (i, j) \in E, \\ 0 & otherwise. \end{cases} \tag{2.1}$$

The degree of a node k_i, is the number of nearest-neighbor connections that the node i has. The consideration of the elongation of the unit rectangles where the nodes of the graph reside is an important modeling feature in the current work. There has been experimental evidences that the elongation of the plots and fields in which the plants are growing decreases the rate of epidemic propagation and makes more difficult the infection to become an epidemic. However, it is obvious that the elongation of the rectangles with a fixed connection radius will make the graph disconnected at certain point. In the general case of RRGs we have proved that the average degree $\bar{k}$ depends on the number of nodes n and a function f of the elongation of the rectangle: $\bar{k} = (n - 1)f$, where f is given by (see ref. Estrada and Sheerin (2015) for details):

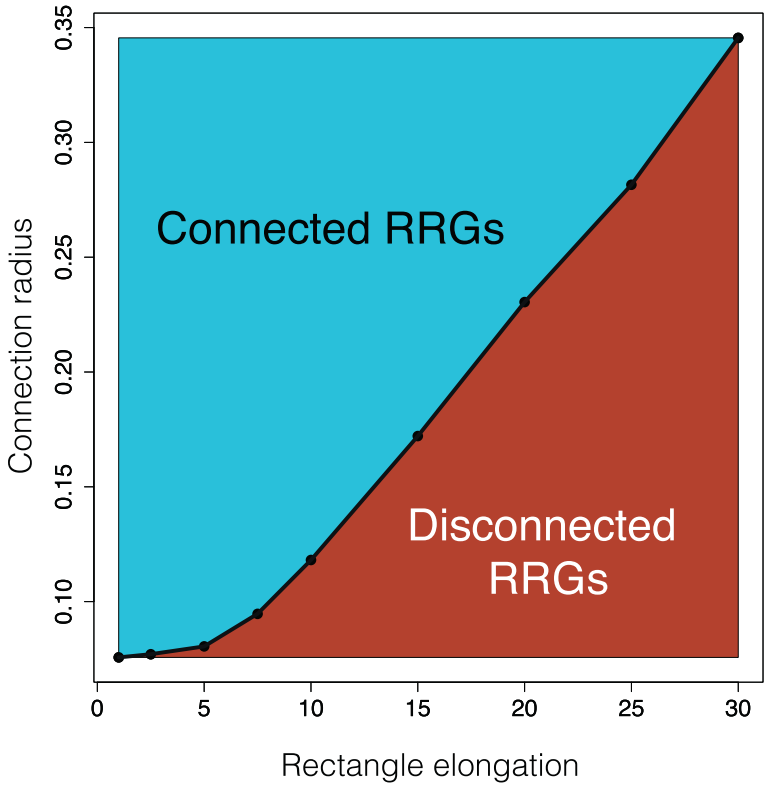

Fig. 2. Plot of the connectivity radius versus the rectangle elongation for the RRGs. The line dividing the two regions represents the connectivity radius values of radius and elongation for RRGs with $n = 1000$ nodes. All the calculations are the result of averaging 20 random realizations of the RRG with the given parameters.

$$f = \begin{cases} \pi r^2 - \frac{4}{3}(a + a^{-1})r^3 + \frac{1}{2}r^4, & \text{for } 0 \le r \le b \\ -\frac{4}{3}ar^3 - r^2a^{-2} + \frac{1}{6}a^{-4} + (\frac{4}{3}r^2 + \frac{2}{3}a^{-2})\sqrt{a^2r^2 - 1} & \text{for } b \le r \le a \\ \quad +2r^2 \arcsin(\frac{1}{ar}), & \\ -r^2(a^2 + a^{-2}) + \frac{1}{6}(a^4 + a^{-4}) - \frac{1}{2}r^4 & \text{for } a \le r \le \sqrt{a^2 + a^{-2}} \\ \quad +(\frac{4}{3}r^2a^{-1} + \frac{2}{3}a)\sqrt{r^2 - a^2} + (\frac{4}{3}r^2 + \frac{2}{3}a^{-2})\sqrt{a^2r^2 - 1} & \\ \quad -2r^2(\arccos(\frac{1}{ar}) - \arcsin(\frac{a}{r})). & \end{cases} \tag{2.2}$$

Then, in the case of RRGs the probability of the graph being connected depends on both the connection radius and the elongation of the rectangle. Explicitly, such probability $P[\cdots]$ is written in the limit when the number of nodes is very large as

$$\lim_{n\to\infty} P[(n-1)f - \log n \le \alpha] = \exp(-\exp(-\alpha)), \tag{2.3}$$

where α is a parameter, which indicates that when $\alpha \to +\infty$ the RRG is almost surely connected when $n \to \infty$, and almost surely disconnected when $\alpha \to -\infty$. Because the parameter α is unknown and it depends on the specific RRG considered, we have obtained a lower bound for $\exp(-\exp(-\alpha))$ using (2.3):

$$\exp(-\exp(-((n-1)f - \log n))) \le \exp(-\exp(-\alpha)). \tag{2.4}$$

Then, we can plot the values of the connectivity radius versus the elongation of the rectangles (see Fig. 2). The curve joining the points of this plot makes a separation between the RRGs which are connected (upper triangular part) from those which are disconnected (lower triangular part). That is, the curve represents the critical radii versus critical elongation, and it gives the critical region indicating the connectivity of the RRGs. In this work we use values of r which guarantee that the graph is connected for the studied values of the elongation parameter a. In addition, we check individually that every graph is connected. Another important aspect related to the connectivity of RRGs is about network density, i.e., number of links per given size. The number of links varies with the elongation of the rectangle, with larger elongation producing less links for a constant connection radius. In modeling plant diseases we keep the connection radius constant as a consequence of the fact that the radius of action of the pathogen is fixed. Then, the decay of the edge density with the elongation is a natural result due to the fact that the elongation makes the propagation of the pathogen more directional. That is, in a square the pathogen has almost the same probability of hopping in any direction, but in a very elongated plot it can only hops in the direction of the larger axis, and such decrease in the direction of the hopping is reflected in the decay of the number of edges in the graph.

2.2. Long-range interactions (LRI) epidemic models

2.2.1. Generalities

Here we consider two epidemiological models for modeling the disease propagation on plants, namely the SIS and SIR models. When studying plants a frequently found situation is a systemic or

'all-or-nothing' diseases of crops or annual plants. In these cases, the most convenient model to be used is the SIR one, in which the plants are either susceptible, infected or die after the infection. However, in some situations hosts recover from the disease and become susceptible again as soon as they recover. This is the case for instance when plants recover by shedding and regrowing diseased leaves. In this particular scenario the most appropriate model is the SIS, which has been used in such situations by several authors (Aguayo et al., 2014; Bauch, 2005; Bolker, 1999). In the case of vectored plant diseases, such as the ones mainly considered here, Jeger et al. (2011) have recommended the SIS model as the main theoretical framework for modeling the epidemic spreading. We now describe the main mathematical formalism for these two models in which we will incorporate the LRIs.

Let us now write the equations of the SIS model taking place through the nodes and edges of the graph. Let S_i be the probability of individual i of being susceptible to the infection, and let x_i be the probability of individual i of being infective after having been infected by the disease. Then, if the birth and death rates of the epidemics are β and μ, respectively, we have the following equations for the SIS model on the graph:

$$\dot{S}_i = -\beta S_i \sum_j A_{ij} x_j + \mu x_i, \tag{2.5}$$

$$\dot{x}_i = \beta S_i \sum_j A_{ij} x_j - \mu x_i. \tag{2.6}$$

In a similar way, the SIR model is written as:

$$\dot{S}_i = -\beta S_i \sum_j A_{ij} x_j, \tag{2.7}$$

$$\dot{x}_i = \beta S_i \sum_j A_{ij} x_j - \mu x_i, \tag{2.8}$$

$$\dot{R}_i = \mu x_i, \tag{2.9}$$

where R_i is the probability of individual i of being recovered from infection.

2.2.2. LRI on plant diseases

In the previously defined model, an infective particle is considered to jump from one plant i to another plant j if and only if the two plants are connected in the corresponding spatial network. That is, in the case of the RRGs $G = (V, E)$ considered here the transmission of the disease is only possible if $(i, j) \in E$. This scenario corresponds to the case of an insect vector that hops only at short distances without any pre-alignment behavior. That is, this corresponds to an insect that does not discriminate among the different plants around its actual position and simply hops to the nearest neighbor one which is available. This situation is represented in Fig. 3(a).

A different scenario arises if we consider that the insect vector has a pre-alignment behavior and also that it needs a plant contact and assessment of the surface cues after landing. In this case, the insect vector can flight from its current position to another plant, which looks attractive to it, and which is not necessarily close to the current one. Also, it is possible that the nearest plants look attractive or appetitive to the insect, it lands on it, but after probing it decides not to colonize the plant. Then, it hops to another nearest neighbor and the process continues until it finds an appetitive plant. Indeed, Irwin et al. (2007) have identified the following categories of aphids according to their behavior: (a) transient non-vectors, which land and probe but do not colonize the crop and do not transmit the virus; (b) transient vectors, which land and probe without colonizing the crop but transmit the virus; (c) colonizing non-vectors, which land, stay and reproduce on the crop but do not transmit the virus; (d) colonizing vectors, which land, stay and reproduce on the crop and transmit the virus. Obviously, we are interested here in those categories in which there is transmission of the virus, but the category (a) is also important, as it represents a non-steady state of the vector, which can be exploring until it finds the appropriate plant to become any of the other categories. In Fig. 3(b)–(d) we represent scenarios in which an insect vector can hop not to the nearest neighbor of its current position but to a second, third, fourth neighbor, and so forth. In the way they are represented here they intent to capture the idea that the insect can land in a nearest neighbor and probe it but being in category (a) at each of the empty circles of the graphics. For instance, in Fig. 3(b) the insect hops to a nearest neighbor and probe on it but decides not to colonize and hops again to the second nearest neighbor, probes it and decides to colonize it. Then, the resulting trajectory is a two-edges hop in the network, where the transmission is effective only at the endpoints, because at the intermediate ones the insect behaves as a transient non-vector.

Then, in mathematical terms our model consists of the following. We consider that the chances of the virus to be transported from an infected to a susceptible plant decays with the "distance" at which these two plants are located in the field. This is a consequence of the empirical observations that most of insects prefer to colonize not so distant plants from its original position. By distance we consider here the separation in terms of the number of steps in the shortest path connecting both nodes in the network, due to the possible multi-hopping nature of these exploratory hops of transient non-vectors. Resuming, in Fig. 3 an infected plant (represented in light green) can transmit the pathogen to any of its nearest neighbors with a probability σ_1. In addition, the pathogen can jump to a second nearest-neighbor with probability $\sigma_2 < \sigma_1$. Similarly, it can hop to a third, fourth, and so forth neighbor, such that the probabilities decay as: $\sigma_{d_{max}} < \cdots < \sigma_1$, where d_{max} is the diameter—the longest shortest path—of the network.

2.2.3. Mathematical formulation

In order to implement mathematically the model of disease propagation in this new scenario we need to define the d-path adjacency matrices which account for the hop of the infective particle beyond the nearest neighbors from its current position. Let $d_{\max}$ be the graph diameter, i.e., the maximum shortest path distance in the graph.

Definition 1. Let $d \leq d_{max}$. The d-path adjacency matrix, denoted by A_d, of a connected graph of n nodes is the square, symmetric, $n \times n$ matrix whose entries are:

$$A_d(i, j) = \begin{cases} 1 & if\ d_{ij} = d, \\ 0 & otherwise, \end{cases} \tag{2.10}$$

where d_{ij} is the shortest path distance between the nodes i and j. Obviously $A_1 = A$. The d-path degree of the node i is given by

$$k_d(i) = \left(\mathbf{1}^T A_d\right)_i \tag{2.11}$$

where $\vec{1}$ is an all-ones column vector.

Let us now consider the following transformed d-path adjacency matrices:

$$\tilde{A^\tau} = \begin{cases} \sum_{d=1}^{d_{max}} d^{-s} A_d, & \text{for } \tau = \text{Mell},\ s > 0 \\ A + \sum_{d=2}^{d_{max}} \exp(-\lambda d) A_d, & \text{for } \tau = \text{Lapl},\ \lambda > 0, \end{cases} \tag{2.12}$$

where τ indicates the type of transformation, i.e., Mellin or Laplace transforms. In the case of Laplacian operators transformed by the same type of transformation we have previously proved that the

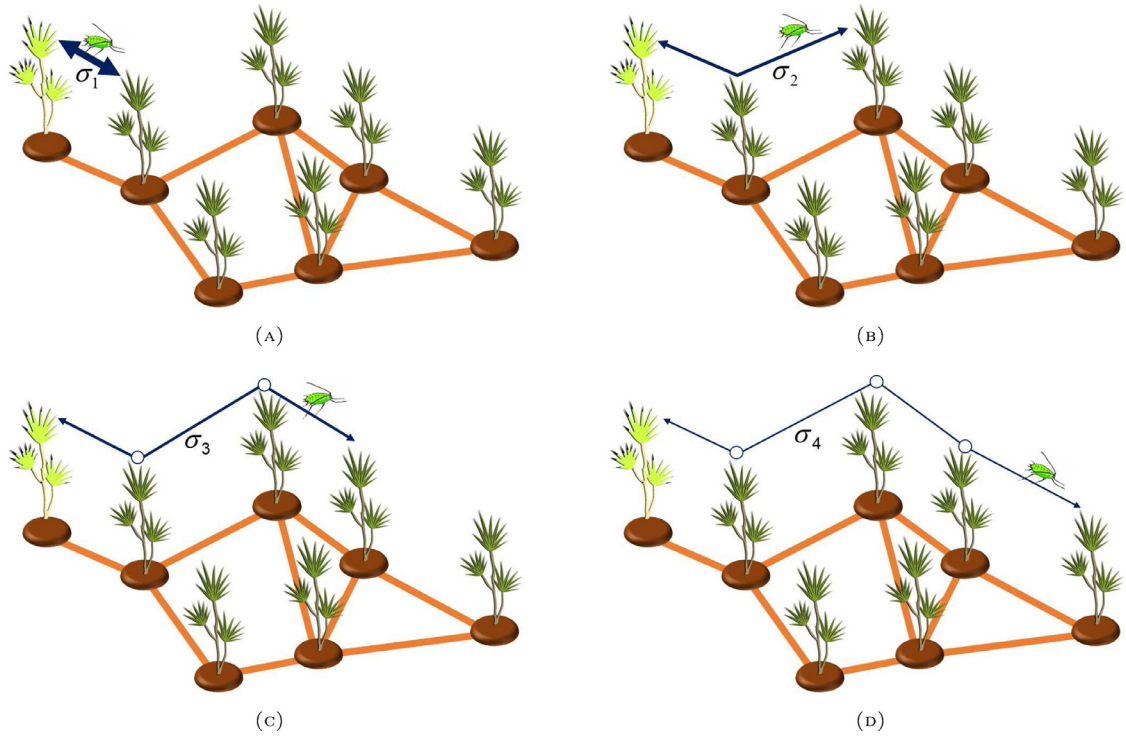

Fig. 3. Schematic representation of the long-range dispersal of pathogens among plants embedded in a field or plot, such that the probabilities of jumping from one plant to another decay with the shortest-path distance among the plants. From (a) to (d) the hop of the pathogen occurs in one, two, three and four steps, respectively, such as it is transported from the first (infected) plant to the last (susceptible) plant but not to any of the intermediate ones (marked by empty circles). The probabilities in which such processes occur decays with the number of steps, such that: $\sigma_4 < \sigma_3 < \sigma_2 < \sigma_1$. (For interpretation of the references to color in this figure legend, the reader is referred to the web version of this article.)

transformed operators are self-adjoint and bounded under certain conditions (Estrada et al., 2017, 2018).

Let us define the generalized degree of a given node i as

$$\tilde{k}^{\tau}(i) = \left(\tilde{A}^{\tau}\mathbf{1}\right)_i. \tag{2.13}$$

Now we plug the transformed d-path adjacency matrices into the SIS and SIR models to get the generalized epidemic models with long-range interactions. These equations are given below for the case of the Mellin transformed d-path adjacency matrices in the SIS model

$$\dot{S}_i = \beta S_i \sum_j \left(\sum_{d=1}^{d_{max}} d^{-s} A_d\right)_{ij} x_j + \mu x_i, \tag{2.14}$$

$$\dot{x}_i = \beta S_i \sum_j \left(\sum_{d=1}^{d_{max}} d^{-s} A_d\right)_{ij} x_j - \mu x_i. \tag{2.15}$$

Then, when $s \to \infty$ we recover the classical SIS or SIR models in which there is no long-range hops of the infective particle. When $s \to 0$ the infective particle can hop to any node of the graph with identical probability, which corresponds to the situation of an infection diffusing on a complete graph K_n. The situation is quite the same with the Laplace transformed d-path adjacency matrices as defined in (2.12) for the cases when $\lambda \to \infty$ and $\lambda \to 0$. Thus, in every case we always recover the original classical epidemiological models of graphs for large values of the parameters in the transforms of the d-path adjacency matrices and we approach the diffusion of the epidemic on a complete graph when these parameters tend to zero.

2.3. Markovian formulation

Eqs. (2.14) and (2.15) are only valid when the number of infected individuals is small, e.g., close to the epidemic threshold. Here, following the framework introduced in Gómez et al. (2010), we formulate a Markovian evolutionary equation that, in principle, is valid for any epidemic prevalence. We denote, as in the former section, β as the probability that a susceptible node contracts the disease when contacting an infected one, and μ the probability that an infected node passes to Susceptible (SIS) or Recovered (SIR). Let $p_i(t)$ be the probability that a node i is infected at time t. This way, under the framework of an SIS disease, the evolution of this probability reads:

$$p_i(t+1) = p_i(t)(1-\mu) + (1 - p_i(t))q_i(t)\,, \tag{2.16}$$

where the first term on the r.h.s accounts for the probability that if node i is infected at time t it will not recover in the next time step $t+1$. The second term in its turn, is the probability that, when node i is healthy at time t, it becomes infected at time $t+1$, being the infection probability $q_i(t)$. This probability reads:

$$q_i(t) = 1 - \prod_{j=1}^{N} \left[1 - \beta \tilde{A}^{\tau}_{ij} p_j(t)\right] \tag{2.17}$$

where matrix $\tilde{A}^{\tau}$ accounts for the interaction strength between pairs of nodes as defined in Eq (2.12). The expression $q_i(t)$ is calculated as 1 minus the probability that the node i is not infected by any infectious contact. This last probability is the product over all the possible contacts of node i, considering that a node j transmits the disease to i with probability $\beta \tilde{A}^{\tau}_{ij} p_j$. Note that if node j is not connected to i, $\tilde{A}^{\tau}_{ij} = 0$, then the corresponding term in the product is equal to 1, since j cannot infect i regardless of its state, $p_j(t)$.

Eq (2.16) governs the evolution of a SIS epidemics. For an SIR disease the Markovian equations reads as follows:

$$p_i(t+1) = p_i(t)(1-\mu) + (1 - p_i(t) - \rho_i(t))q_i(t) \,, \tag{2.18}$$

$$\rho_i(t+1) = \rho_i(t) + \mu\, p_i(t) \,, \tag{2.19}$$

where $\rho_i(t)$ is the probability that node i is recovered at time t. The expression for the infection probability $q_i(t)$ is identical to that of Eq (2.17).

We should notice here that, as explained before, these equations hold for any disease incidence, while Eqs (2.14) and (2.15) are only valid when the disease prevalence is small. To explain this, take Eq (2.17) for $q_i(t)$ and consider that the prevalence is small, $p_i \ll 1 \ \forall i$, and for this reason let us denote $p_i = x_i$. Then, the product in (2.17) transform into: $1 - \sum_{j=1}^{N} \beta \tilde{A}^{\tau}_{ij} x_j$. Introducing the new expression for $q_i(t)$ in Eq (2.18), and passing from discrete to continuous time, we recover a similar expression to that in Eq (2.15) for the evolution of the infected state of node i. For more details the reader is referred to Gómez et al. (2011).

2.4. LRI epidemics vs. dispersal kernel models

Arguably, the most used models for the study of dispersal processes in ecology are based on "dispersal kernels", a term which emerges from the mathematical studies of population spread. Dispersal kernels are widely applied to the study of effective dispersal in plant studies, such as seedlings and sapling, as well as in effective pollen dispersal and the dispersal of active movers (Nathan et al., 2012). In general, a dispersal kernel consists in a single point source designated as the origin of the dispersion embedded into a continuous space. It is assumed that the population of dispersers follows a given probability density function (PDF), which is named the dispersal location kernel and denoted by $K_L(r)$. Then, the probability of having a dispersal end point with given coordinates (typically in polar coordinates) in an infinitesimally small area $dA = dxdy$ (see Fig. 4) is obtained from that PDF as $K_L(r)dA$. In general, it is assumed that the dispersal shows radial symmetry, such as the kernel integrates to 1 over the whole two dimensional space. Nathan et al. (2012) have reviewed 13 different types of dispersal kernels, such as Gaussian, negative exponential, power-law, logistic, etc. The applications reported for these kernels include the dispersal of pollen, seeds, beetles, moths, birds, mammals, butterflies, fish, propagules, and flies, with pollen and seedling having the largest number of reports. Then, there is a fundamental difference between the use of dispersal kernels and the LRI epidemic model developed here. Dispersal kernels are appropriate for modeling processes in which the spread is produced on a continuous space, such as the case of pollen, seeding or the radial distribution of insects mainly driven by wind. However, in the case of insect vectors the situation is greatly different due to the behavioral events that precede the transmission of the viruses. For instance, it is reported that the flight of whiteflies in the field is not entirely wind-oriented, possibly due to the fact that they are looking for the most attractive and appetitive plants. The documented fact that even after landing aphids may or may not colonize and transmit the viruses to a plant also imposes certain differences with the use of dispersal kernels. Indeed, in the LRI epidemic model we have a discrete space in which the plants are represented at specified positions of the space. We also assume that the propagator of the disease hops from plant to plant as it is characteristics of insect vectors.

In the particular case of insect vectors like aphids it should be noticed that there are two main propagation mechanisms, either through "inadvertent" or "intentional" transport mechanisms (Fereres et al., 2017). The first corresponds to the case in which aphids are transported in an involuntary act, such as when they are propelled by the force of impact, gravity, air current, of a combination of them. The intentional transport is a voluntary act which is prompted by the preprogrammed movement of the aphids–the most important one being migration–or by external perturbations in which the aphids are driven by their sensed stimuli to the environment. The class of inadverted transport is clearly well-described by dispersal kernels due to the spatial characteristics of the processes involved. On the other hand, the intentional displacement is much better described by LRI on networks as described here. Thus, we think that both models (dispersal kernels and LRI epidemic) are complimentary more than duplicative. It is true that if the density of the plant population is very high, covering mainly the whole 2D space, then both approaches are appropriate for describing the dispersal of pathogens across the plants. It is also important to remark that the LRI epidemic model can be enriched by using many of the different types of functions already used as dispersal kernels instead of the only two ones that we have used here. Finally, it should be remarked that extensions of the current approach by combining it with dispersal kernels will offer a gold opportunity to describe transport of insect vectors due to inadverted and intentional mechanisms combined.

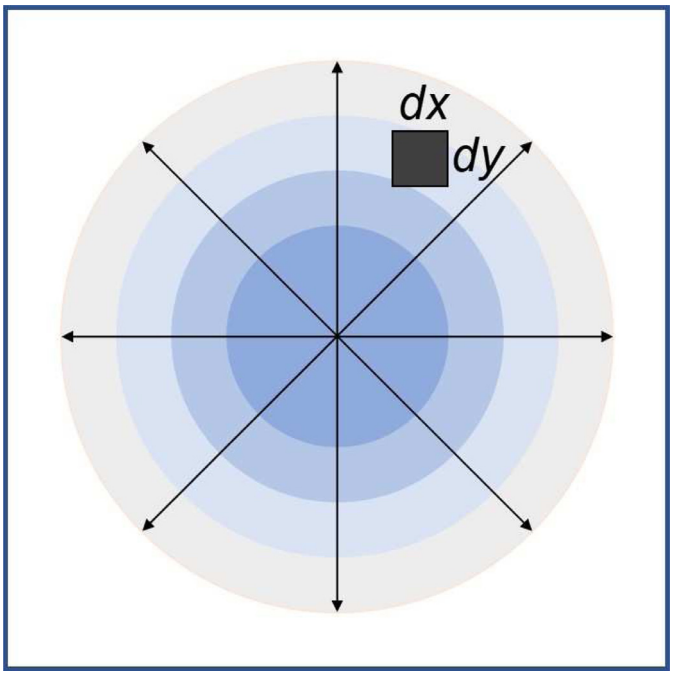

Fig. 4. Illustration of a dispersal kernel with origin in the center of coordinates and a small region of area $dA = dxdy$ for which the probability of finding the disperser is given by $K_L(r)dA$, where $K_L(r)$ is the dispersal location kernel.

3. Results

Let us now analyze what are the effects of considering long-range interactions in a population subjected to contagion processes of SIR and SIS types. To this aim we build synthetic networks by first constructing a RRGs with $a = 2$ and $r = 0.1$. With the adjacency matrix A_1 of the graph we calculate the different distance matrices A_d in order to construct both the Mellin and Laplace transformations of the graph corresponding to different values of s, as introduced in Eq (2.12). Once the networks are built and matrices $\tilde{A^{\tau}}$ computed, we conduct extensive numerical Monte Carlo simulations of both the SIS and SIR dynamics and for different values of the transformations parameters. In the simulations we start seeding the infection in a small fraction, 0.01, of the nodes. Here

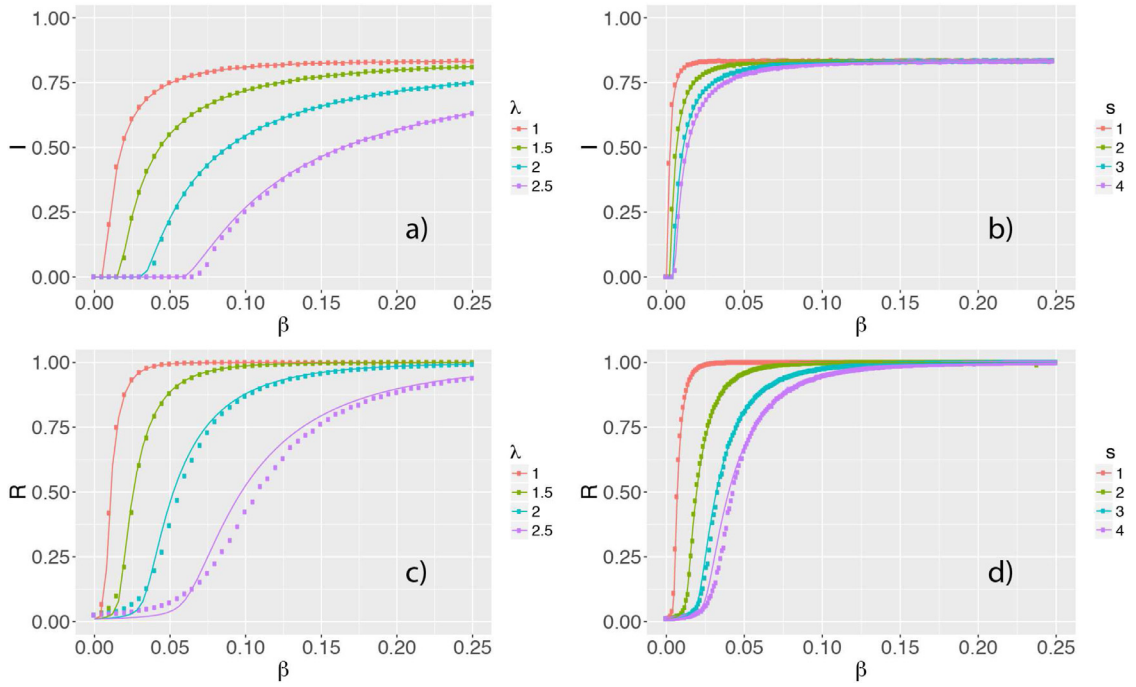

Fig. 5. Comparison between the numerical solution of the Markovian formulation and the Monte-Carlo simulations for the SIS ((a) and (b)) and SIR ((c) and (d)) dynamics and for the Exponential ((a) and (c)) and Mellin transformations ((b) and (d)). Continuous lines represent the Markovian formulation while colored circles Monte-Carlo simulations. Different colors represent the different parameters of the transformations. Each point is the average over 500 Monte-Carlo simulations with different initial conditions. The original network is a RRG with $n = 10^3$ nodes, elongation $a = 2.0$ and connection radius $r = 0.1$. (For interpretation of the references to color in this figure legend, the reader is referred to the web version of this article.)

we always use discrete time step simulations. At each time-step, each infected node contacts all the susceptible agents in the network and the disease is propagated with probability $A_{ij}^{\tau}\lambda$ –where A_{ij}^{τ} is the interaction strength between nodes i and j – and then, all the nodes update their state synchronously. In the SIS we let the system evolve for $5 \cdot 10^4$ time-steps to assure that the steady state has been reached and then, wait for an additional 10^3 time-steps to calculate the fraction of infected nodes I as the average of $I(t)$ over this last period. In the SIR dynamics instead, we let the system evolves until the epidemics ends and thus calculate the fraction of recovered (dead or removed) nodes R. For each selection of the transformation's parameters and infectivity λ we perform 500 independent runs with different initial conditions. The final values of I and R are obtained as the average over all the runs. For the Markovian formulation of the two dynamics the epidemic curve has been obtained iterating for the nodes in the system of Eqs. (2.16) and (2.17) for the SIS and Eqs. (2.18) and (2.19) for the SIR respectively. Using a RRG composed by $n = 10^3$ nodes and elongation $a = 2.0$ ($r = 0.1$) we compare the results of the Markovian formulation and the numerical simulations for the four possible cases: SIS and SIR dynamics, Exponential and Mellin transformations. For all the panels of Fig. 5 we have a good agreement between the Markovian (continuous lines) and numerical Monte Carlo simulations (circles).

3.1. Influence of long-range dispersal

As expected, in all the scenarios a decrease in infected and dead plants is observed for higher values of the transformations parameters – i.e., lower interaction strength between distant nodes – highlighting the role of physical distance between infected plants. Another interesting result of our analysis is that the Mellin transformation favors more the diffusion of the disease with respect to the Laplace transformation (see Fig. 5). These differences are very important in practical terms. It is known that when dispersal processes are described by exponentially decaying distributions (Scherm, 1996), the probability of moving a given distance decreases with the separation of the places at least in proportion to the exponential distribution. These models can be approximated by diffusion models on an appropriate scale. In recent years, there has been accumulated evidence on the existence of unusual, extreme dispersal events, which are better modeled by power-law decay dispersal than with exponential ones. The spatial consequences of this kind of dispersal processes are analyzed in a further section of this paper.

A very important observation is that when the transformation parameters λ or s tend asymptotically to zero, i.e., when the long-range dispersal is quite strong, the epidemic threshold goes to zero. That is, as the long-range dispersal of the pathogen increases the number of infected plants needed to trigger an epidemics is practically nil. The *epidemic threshold* $\zeta = (\frac{\beta}{\mu})$ represents a threshold in the sense that when $\zeta < 1$ the infection dies out and if $\zeta > 1$ the disease becomes an epidemic. In those cases where $\zeta = 1$, the disease remains in the population becoming endemic. The value of this threshold strongly depends on the topology of the network. In particular, for a given graph $G = (V, E)$, it has been shown that (Chakrabarti et al., 2008; Gómez et al., 2010; Van Mieghem et al., 2009):

$$\zeta = \frac{1}{\ell_1(G)}, \tag{3.1}$$

where $\ell_1(G)$ is the largest eigenvalue of the adjacency matrix of the network. Then, let $\tau = \{\lambda, s\}$ be the parameter of the transform used in the SIS or SIR model described in this work. We then have the following result.

Lemma 2. *Let $G = (V, E)$ be any graph with n nodes and with transformed d-path adjacency matrix A^{τ} for $\tau = \{\lambda, s\}$. Let $\zeta(\tau) = (\lambda_1(G, \tau))^{-1}$ be the epidemic threshold and $\lambda_1(G, \tau)$ be the largest*

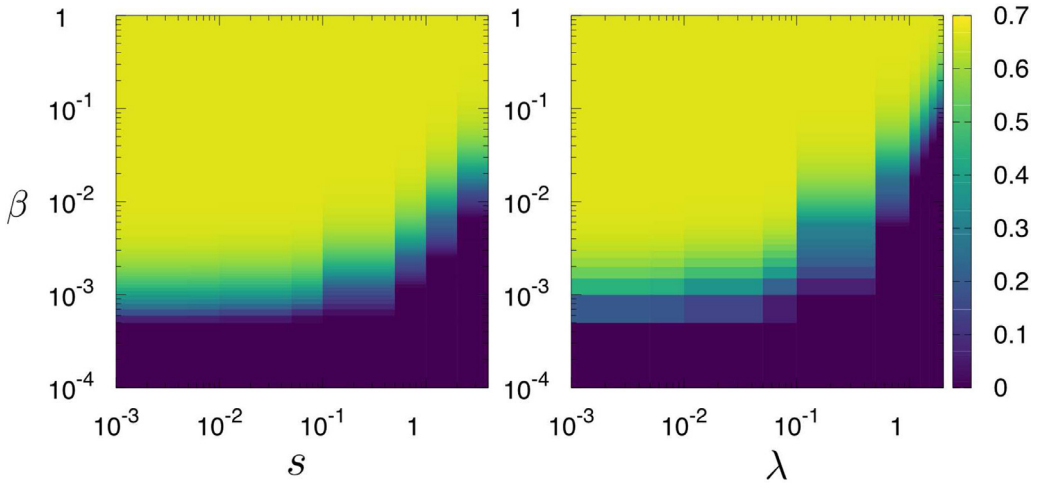

Fig. 6. The panels show (see color code) the stationary fraction of infected individuals in the Markovian dynamics of the SIS model as a function of the infection probability β and the exponents, s (Mellin) and λ (Laplace), of the transformations at work. The recovery probability has been set to $\mu = 0.5$ and the size of the network is $n = 10^3$. (For interpretation of the references to color in this figure legend, the reader is referred to the web version of this article.)

eigenvalue of $\tilde{A^{\tau}}$. *Then,*

$$\lim_{n\to\infty}\lim_{\tau\to 0}\zeta(\tau) = 0. \tag{3.2}$$

Proof. We have that $\lim_{\tau\to 0}\tilde{A^{\tau}} = J - I$, where J is an all-ones matrix and I is the corresponding identity matrix. Then, $\lim_{\tau\to 0}\lambda_1(G,\tau) = \lambda_1(J-I) = n-1$, where n is the number of nodes. Thus, for sufficiently large graphs, i.e., $n\to\infty$ we have that $\lim_{n\to\infty} 1/(n-1) = 0$, which proves the result. □

In other words, for sufficiently large graphs and with very strong long-range dispersal of the pathogen, the number of infected individuals needed to trigger an epidemics is negligible. In addition to the Montecarlo simulations we have solved the Markovian equations for the SIS model. In Fig. 5 we show the good agreement between the Markovian approach and the results of the Monte Carlo simulations. The main advantage of the Markovian approach is that we do not need to perform many computational realizations. Instead, we only solve the equations once for each λ value. The two panels of Fig. 6 show (in color code) the fraction of infected individuals for the SIS model, as a function of the infection probability β and the exponents of the respective transformations s (Mellin) and λ (Laplace). The number of infected individuals is calculated here as $I = \sum_{j=1}^{N} p_j$ in the stationary state. The results clearly show that as exponents s and λ approach to zero (note the logarithmic scale in the axes of both figures) the critical infectivity β_c (i.e. the value of β for which $\zeta = 1$) gets smaller. Obviously, as these exponents become very small we reach a saturation for the epidemic threshold around a small value $\beta_c \sim 10^{-3}$ due to the finite size of the networks $n = 10^3$.

3.2. Influence of plot/field elongation

One of the most important characteristics of the current model is that we can study the influence of the elongation of plots and fields over the propagation of a disease on plants. That is, using the random rectangular graphs instead of the classical "RGG" we can elongate the rectangle keeping the area of the plot/field constant. We investigate the effects of this rectangle elongation by studying the epidemic dynamics on rectangles with length to width ratios ranging from 1 to 100. In Fig. 7 we illustrate the results of applying the Laplace transform to the SIR model using different values of the transform parameter λ and for different elongations of the rectangle. As can be seen, for any value of the Laplace transform parameter λ there is a significant influence of the rectangle elongation of the spread of the disease. The main effect observed is a decay in the speed of propagation of the disease as a function of β as observed by the smaller percentage of dead plants R when the rectangle has a width/length ratio of 100 than when it has a ratio of 1. The effect of larger λ is observed across the panels as a result of the delay in reaching the saturation of the epidemic as a function of β. In Fig. 8 we illustrate the results obtained for the elongation of rectangles with width/length ratios from 1 to 100 when the dynamics is controlled by a Mellin transform of the SIR model. In general, the results are qualitatively similar to those obtained by the Laplace transform, but there are significant quantitatively differences which deserve to be considered in detail. Let us first consider the effect of the infectivity β. It can be seen that the Mellin transformed dynamics reaches the saturation for smaller values of the infectivity β than the Laplace transformed dynamics. For instance, even when the Mellin parameter is relatively large, e.g., $s = 4$, the saturation is reached for relatively small values of β (see panel (d) of Fig. 8). However, this is not observed for the Laplace transform where even for relatively small values of λ the saturation is obtained for relatively large values of the infectivity (see panels (c) and (d) of Fig. 7). This is a consequence of the following. In the Mellin transform we have a power-law dependence of the pathogen jumps which make that it can reach regions very far from its original position in the plot/field. Such hops are not so dramatic in the case of the Laplace transformed one, where the jumps are controlled by an exponential law.

Now, the most remarkable, and surprising, effect of elongation is observed when we consider its effects on the percentage of plant dead for a given infectivity value. In the case of the Laplace transform when the long-range dispersal is very strong, e.g., $\lambda = 0.5$ the elongation of the rectangle from $a = 1$ to $a = 10$ drops the percentage of deaths by 25%. However, in the case of the Mellin transformed dynamics when the long-range dispersal is quite strong, e.g., $s = 1$, the percentage of deaths is dropped by 50% when the rectangle is elongated from $a = 1$ to $a = 10$. This result is at first unexpected and somehow counter-intuitive because the effects of the long-range dispersal produced by the Mellin transformed dynamics are stronger than those produced by the Laplace transform. Thus, we should expect that the percentage of deaths in the Mellin transformed dynamics for any rectangle should be larger than those produced by the Laplace transformed. However, we

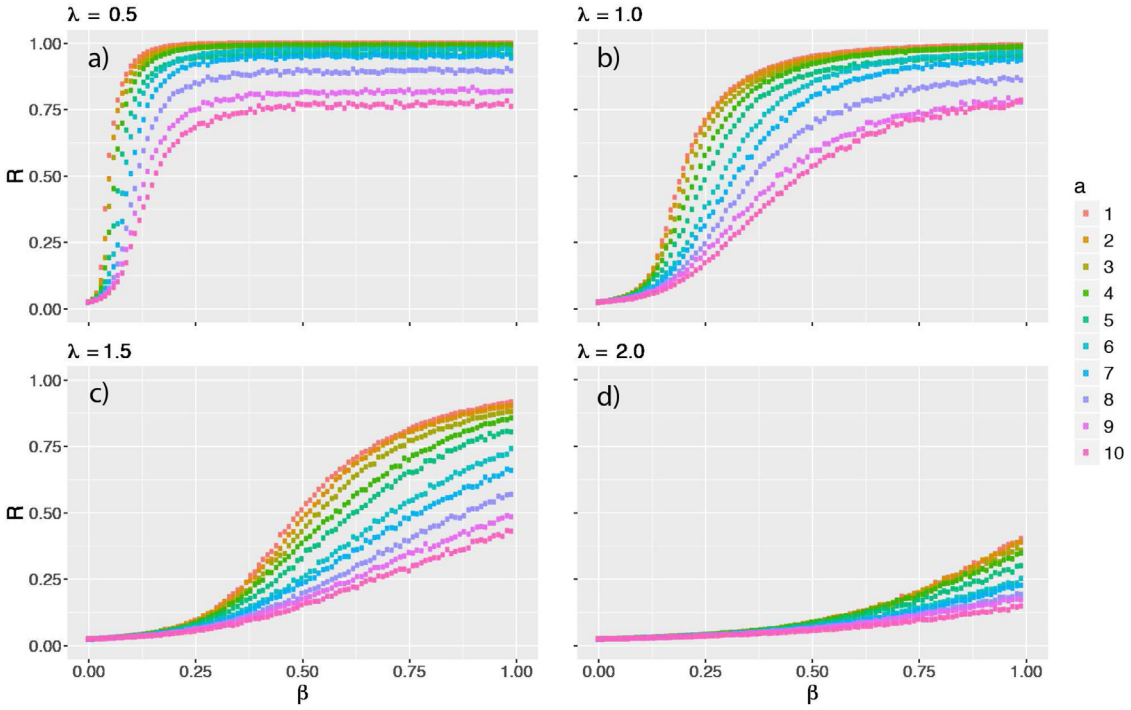

Fig. 7. Effect of elongation a on the final fraction of recovered nodes in the SIR dynamics for 4 different values of the exponential transformation: $\lambda = 0.5$ (panel a), $\lambda = 1.0$ (panel b), $\lambda = 1.5$ (panel c) and $\lambda = 2.0$ (panel d). Each point is the average over 500 Monte-Carlo simulations with different initial conditions. The original network is an RRG with $n = 10^3$ nodes, elongation $a = 1, \ldots, 10$ and connection radius $r = 0.1$.

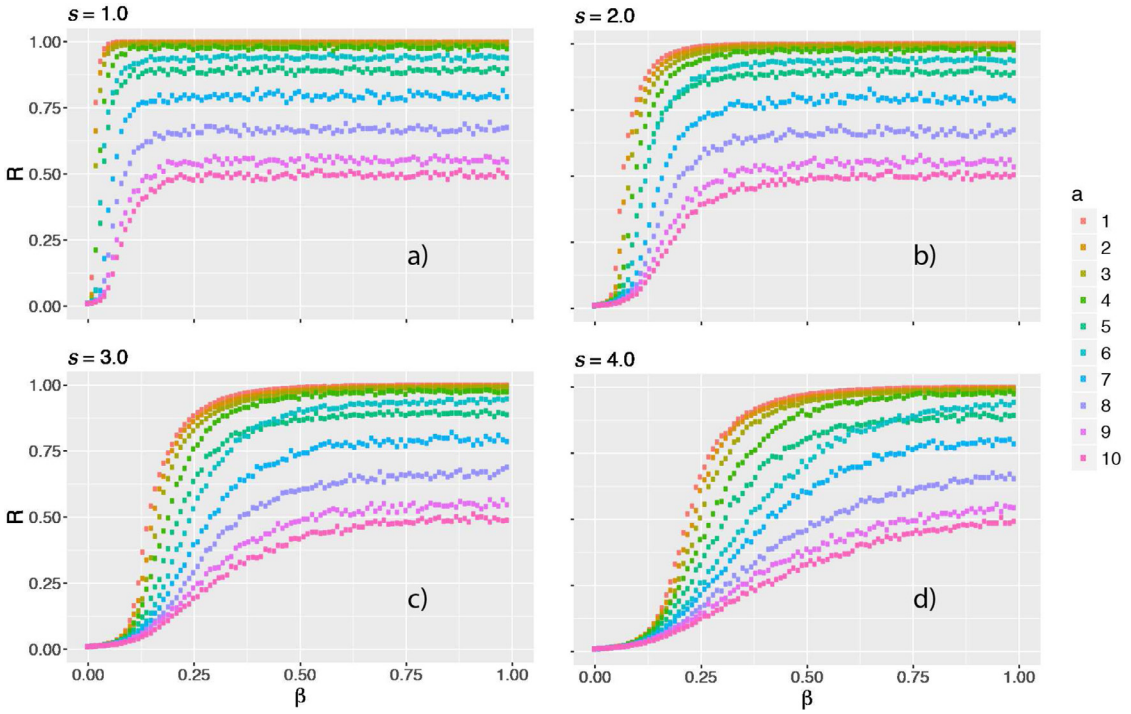

Fig. 8. Effect of elongation a on the final fraction of recovered nodes in the SIR dynamics for 4 different values of the Mellin transformation: $s = 1.0$ (panel a), $s = 2.0$ (panel b), $s = 3.0$ (panel c) and $s = 4.0$ (panel d). Each point is the average over 500 Monte-Carlo simulations with different initial conditions. The original network is an RRG with $n = 10^3$ nodes, elongation $a = 1, \ldots, 10$ and connection radius $r = 0.1$. We have set here $\mu = 0.5$ since we are not trying to characterize any particular disease. For $\mu = 1$, for instance, the recovery is too fast to see the spatial propagation and, conversely, in the case $\mu = 0$ the dynamics would be an SI dynamics. We decided to lie between these two limiting cases.

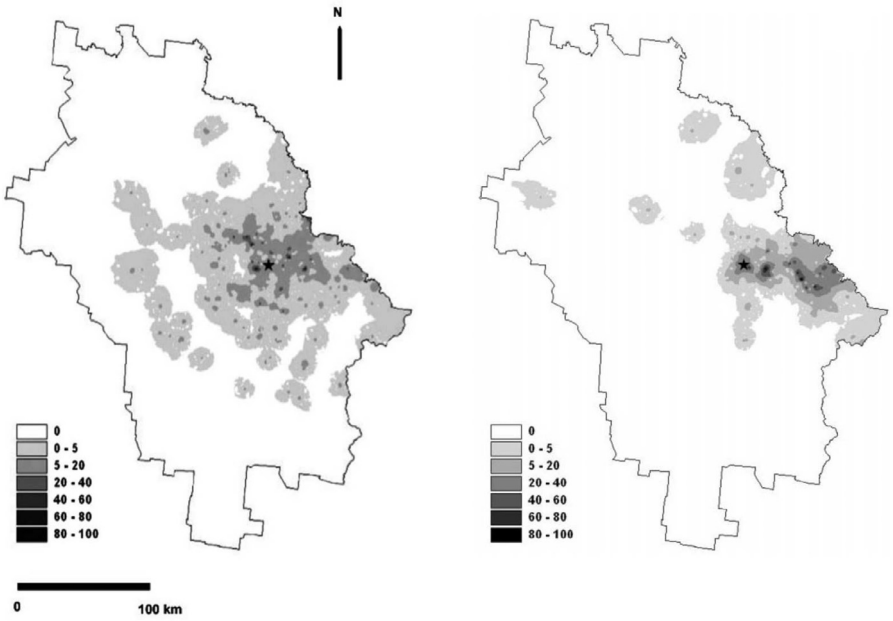

Fig. 9. Abundance (% cover) of (left panel) *C. grandiflora* and (right panel) *Z. mauritiana* in Dalrymple Shire, northern Queensland, Australia (reproduced from (Grice et al., 2000)). The star indicates the site of first introduction. Notice the patchy areas of "infection" and the lack of a clear front wave from the site of first introduction to the uninfected region. Reproduced with permission from Grice et al. (2000).

would notice that we are comparing two transformations (Laplace with $\lambda = 0.5$ and Mellin with $s = 1$) without taking any point in common such as, e.g., the total strength of the interactions (that could be measured as the sum over the entries of the transformed adjacency matrix given two values of λ and s). The main causes of this effect observed here are not totally clear. However, we guess that they should revolve around the fact that the Mellin transformed dynamics produces a much faster propagation of the pathogen across vast regions of the plot/field (see further analysis in the next section). Then, due to the eventual death of the plants in those isolated regions there are not infected plants to continue the propagation and the epidemics eventually dies. The existence of such patches of infection are made clear in the next section of this work.

In closing, we have that the elongation of the plots/fields produces the following effects: (i) the level of infectivity β needed to trigger the epidemics is larger for more elongated rectangles than for the square; (ii) the number of deaths is larger in the square than in the most elongated rectangles; and (iii) the number of deaths is significantly smaller when the dynamics is controlled by the Mellin transform than with the Laplace transform.

3.3. Spatial patterns

An important experimental observation about the dispersal of diseases in plants is the existence of unusual, extreme dispersal events, which follow power-law decay dispersal. The most important consequence of these kinds of dispersal processes of pathogens is the generation of spatial patterns without well-defined epidemic fronts (Shaw, 1995), which generate clusters of different sizes (Filipe and Maule, 2004). This is a fundamental difference with the Gaussian-like diffusive processes in which waves separating infected from uninfected territory exist, such that the first propagate smoothly and at constant speed (Anderson et al., 1986; Van den Bosch et al., 1988; Mollison, 1977). As a matter of example we reproduce here a Figure from (Grice et al., 2000) in which the abundance of *C. grandiflora*–an invasive species, acting here as the pathogen–in Dalrymple Shire, northern Queensland, Australia displays a clear patchy pattern (Fig 9), characteristic of this type of power-law dispersal in the continuous space. The question is then, whether such patchy patterns are also observed in the discrete space in which the LRI epidemic model is developed. Our model clearly reproduces such kind of patchy dispersal of the pathogen in which there is not a clear wave separating infected from uninfected territory. In Fig. 10 we display the dispersal patterns of a pathogen in a rectangular plot of length/width ratio 4 showing the infection times τ_i for $\mu = 0.5$ and $\beta = 0.18$ when starting the simulation from a single infected node which is placed in the top left part of the field. Three cases are shown: (top): the original (not transformed) network; (central): The Mellin-transformed network with $s = 3$; and (bottom): The Laplace-transformed network with $\lambda = 1$. The values of the transformation and β have been chosen since the two transformed networks yield similar number of deaths at the end of the simulation. From the first plot it is clear that for $\beta = 0.18$, the original network is supercritical and the infection pattern is well described as a cascade of infections very well correlated with the spatial distribution of nodes. The second plot (Mellin) shows that the transformed network yields a completely different behavior. First, a large number of deaths for the same β value in a shorter time (30 time steps). This is due to the long-range initial infections (see circles) that appear far away from the first infection seed. The third plot (Laplace) shows that despite the same number of infections are achieved, the mechanisms behind them are quite different. First, there are not significant long-range infections and, second, the time needed is much longer than for the Mellin-transformed network. From these plots we can hypothesize that the patchy behavior is easier to achieve from the Mellin mechanism than for the Laplace one. Indeed, for smaller (although supercritical) β values, most of the realizations of the SIR dynamics in Mellin-transformed networks yield patchy distributions of dead nodes as those found in real scenarios.

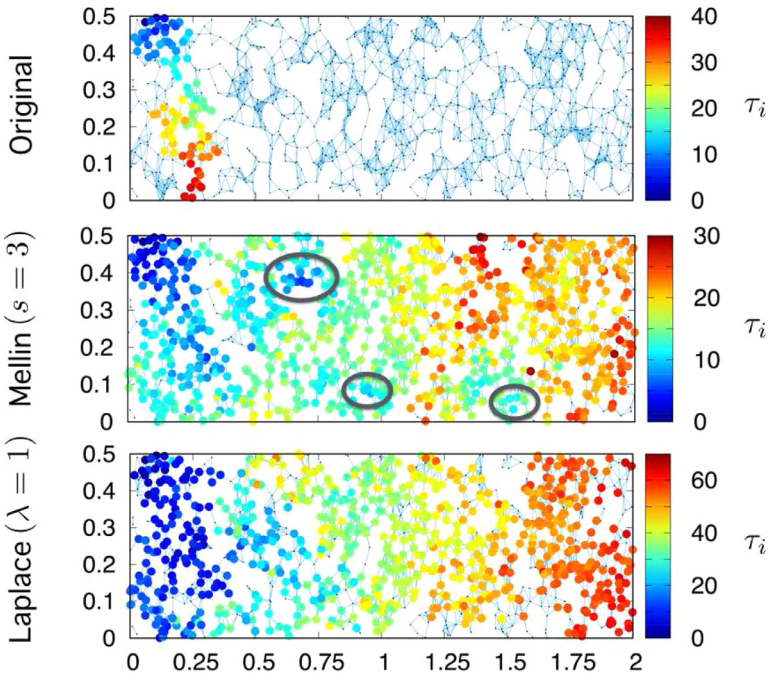

Fig. 10. Time of infection of individual nodes in a RRG with $a = 2$, $n = 1000$, using the non-transformed model (top panel), Mellin-transformed (central panel) and Laplace-transformed (bottom panel) SIR model with $\beta = 0.105$ and $\mu = 0.5$. Here we used $r = 0.05$ to create a sparser networks that allow to visualize better the patchy regions. (For interpretation of the references to color in this figure legend, the reader is referred to the web version of this article.)

4. Conclusions

We have developed a model here that accounts for long-range dispersal of pathogens in disease propagation in networked systems. The model is a generalization of the classical SIS and SIR equations on networks by using a transformed adjacency operator. The current model also incorporates spatial characteristics of the plots and fields in which the plants are embedded. These spatial characteristics are included through the use of random rectangular graphs which allow to consider the effects of the elongation of plots and fields on epidemic spreading dynamics. Using this generalized model we have studied the propagation of epidemics on plants emulating a few realistic scenarios of plant diseases. We have found that under the influence of long-range dispersal there is much faster propagation of a disease than in normal diffusive regimes. We also observed that the elongation of plant plots/fields increases the infectivity needed to trigger the epidemics and that such elongation of the plots/fields decreases dramatically the number of plants dead. That is, the number of plants dead in a very elongated plot/field is much less when the dynamics is controlled by a Mellin transform than when it is controlled by the Laplace one, and they both are significantly smaller than when the disease is propagated without long-range dispersal effects. Last but not least, we also observed that the dynamics in the Mellin-transformed networks is characterized by the existence of patchy regions of infected plants and by the absence of a clear propagation front that separates infected from noninfected plants. All in all, we consider that the current model represents an important step forward for modeling epidemic propagation on plants allowing the variation of a few parameters that simulate realistic scenarios. The model can also be adapted to other scenarios of propagation and dispersal in spatially embedded regions, such as seed dispersal, and propagation of wildfires.

Acknowledgments

JGG acknowledges support from MINECO through grants (FIS2014-55867-P and FIS2017-87519-P) and from the Departamento de Industria e Innovación del Gobierno de Aragón and Fondo Social Europeo (FENOL group E-19). SM is supported by MINECO through the Ramón y Cajal program. EE thanks the Royal Society of London for a Wolfson Research Merit Award.

References

Aguayo, J., Elegbede, F., Husson, C., Saintonge, F., Marçais, B., 2014. Modeling climate impact on an emerging disease, the phytophthora alni-induced alder decline. Global Change Biol. 20, 3209–3221.
Allen, L., Ernest, R., 2002. The impact of long-range dispersal on the rate of spread in population and epidemic models. IMA Vol. Math. Appl. 125, 183–198.
Anderson, R., Mollison, D., Bartlett, M., Southwood, R., 1986. Modelling biological invasions: chance, explanation, prediction: discussion. Phil. Trans. R. Soc. London B 314, 692–693.
Aylor, D., 2003. Spread of plant disease on a continental scale: role of aerial dispersal of pathogens. Ecology 84, 1989–1997.
Bauch, C., 2005. The spread of infectious diseases in spatially structured populations: an invasory pair approximation. Math. Biosc. 198, 217–237.
Bolker, B., 1999. Analytic models for the patchy spread of plant disease. Bull. Math. Biol. 61, 849–874.
Bollobás, B., 1985. Random Graphs. Academic Press, New York.
Bonnot, F., De Franqueville, H., Lourenço, E., 2010. Spatial and spatiotemporal pattern analysis of coconut lethal yellowing in mozambique. Phytopathology 100, 300–312.
Brown, J., Hovmø ller, M., 2002. Aerial dispersal of pathogens on the global and continental scales and its impact on plant disease. Science 297, 537–541.
Campbell, C., Madden, L., 1990. Introduction to Plant Disease Epidemiology. John Wiley & Sons.
Chakrabarti, D., Wang, Y., Wang, C., Leskovec, J., Faloutsos, C., 2008. Epidemic thresholds in real networks. ACM Trans. Inf. Syst. Secur. 10, 1–26.
Clark, J., 1998. Why trees migrate so fast: confronting theory with dispersal biology and the paleorecord. Am. Nat 152, 204–224.
Clark, J., Silman, M., Kern, R., Macklin, E., HilleRisLambers, J., 1999. Seed dispersal near and far: patterns across temperate and tropical forests. Ecology 80, 1475–1494.
Cunniffe, N., Cobb, R., Meentemeyer, R.K., Rizzo, D.M., Gilligan, C.A., 2016. Modeling when, where, and how to manage a forest epidemic, motivated by sudden oak death in california. Proc. Nat. Acad. Sci. USA 113, 5640–5645.

Cunniffe, N., Koskella, B., Metcalf, C., Parnell, S., Gottwald, T., Gilligan, C., 2015. Thirteen challenges in modelling plant diseases. Epidemics 10, 6–10.
Dall, J., Christensen, M., 2002. Random geometric graphs. Phys. Rev. E 66, 016121.
Davis, J., 1987. Modeling the long-range transport of plant pathogens in the atmosphere. Ann. Rev. Phytopathol. 25, 169–188.
Dybiec, B., Kleczkowski, A., Gilligan, C., 2009. Modelling control of epidemics spreading by long-range interactions. J. R. Soc. Interface 6, 941–950.
Estrada, E., Chen, G., 2015. Synchronizability of random rectangular graphs. Chaos 25, 083107.
Estrada, E., Hameed, E., Hatano, N., Langer, M., 2017. Path laplacian operators and superdiffusive processes on graphs. i. one-dimensional case. Lin. Algebra Appl. 523, 307–334.
Estrada, E., Hameed, E., Langer, M., Puchalska, A., 2018. Path Laplacian operators and superdiffusive processes on graphs. II. Two-dimensional case. ArXiv preprint arXiv:1802.00719.
Estrada, E., Meloni, S., Sheerin, M., Moreno, Y., 2016. Epidemic spreading in random rectangular networks. Phys. Rev. E 94, 052316.
Estrada, E., Sheerin, M., 2015. Random rectangular graphs. Phys. Rev. E 91, 042805.
Estrada, E., Sheerin, M., 2016. Consensus dynamics on random rectangular graphs. Physica D 323, 20–26.
Fereres, A., Irwin, M.E., Kampmeier, G.E., 2017. Aphid movement: process and consequences. In: Clobert, J., et al. (Eds.), Dispersal Ecology and Evolution, Second Edition. Oxford University Press, pp. 196–224.
Fereres, A., Moreno, A., 2009. Behavioural aspects influencing plant virus transmission by homopteran insects. Virus Res 141, 158–168.
Ferrandino, F., 2005. The explicit dependence of quadrat variance on the ratio of clump size to quadrat size. Phytopathology 95, 452–462.
Filipe, J., Maule, M., 2004. Effects of dispersal mechanisms on spatio-temporal development of epidemics. J. Theor. Biol. 226, 125–141.
Fleming, R., Marsh, L., Tuckwell, H., 1982. Effect of field geometry on the spread of crop disease. Protection Ecology (Netherlands).
Gilbert, E., 1959. Random graphs. Ann. Math. Stat. 30, 1141–1144.
Gillespie, R., Baldwin, B., Waters, J., Fraser, C., Nikula, R., Roderick, G., 2012. Long-distance dispersal: a framework for hypothesis testing. Trends Ecol. Evol. 27, 47–56.
Gómez, S., Arenas, A., Borge-Holthoefer, J., Meloni, S., Moreno, Y., 2010. Discrete–time markov chain approach to contact-based disease spreading in complex networks. Europhys. Lett. 89, 38009.
Gómez, S., Gómez-Gardenes, J., Moreno, Y., Arenas, A., 2011. Nonperturbative heterogeneous mean-field approach to epidemic spreading in complex networks. Phys. Rev. E 84, 036105.
Gottwald, T., Hughes, G., Graham, J., Sun, X., Riley, T., 2001. The citrus canker epidemic in florida: the scientific basis of regulatory eradication policy for an invasive species. Phytopathology 91, 30–34.
Grice, A., Radford, I., Abbott, B., 2000. Regional and landscape-scale patterns of shrub invasion in tropical savannas. Biol. Invasions 2, 187–205.
Hallatschek, O., Fisher, D., 2014. Acceleration of evolutionary spread by long-range dispersal. Proc. Nat. Acad. Sci. USA 111, E4911–E4919.
Irwin, M., Kampmeier, G.E., Weisser, W.W., 2007. Aphid movement: process and consequences. In: van Emden, H.F., Harrington, R. (Eds.), Aphids as Crop Pests. CAB International, pp. 153–186.
Jeger, M., 1990. Mathematical analysis and modeling of spatial aspects of plant disease epidemics. In: Epidemics of Plant Diseases. Springer Berlin Heidelberg, pp. 53–95.
Jeger, M., Van den Bosch, F., Madden, L., 2011. Modelling virus-and host-limitation in vectored plant disease epidemics. Virus Res. 159, 215–222.
Jeger, M., Pautasso, M., Holdenrieder, O., Shaw, M., 2007. Modelling disease spread and control in networks: implications for plant sciences. New Phytol. 174, 279–297.
Jones, D.R., 2003. Plant viruses transmitted by whiteflies. Eur. J. Plant Pathol. 109, 195–219.
Keeling, M., Woolhouse, M., Shaw, D., Matthews, L., Chase-Topping, M., Haydon, D., Cornell, S., Kappey, J., Wilesmith, J., Grenfell, B., 2001. Dynamics of the 2001 UK foot and mouth epidemic: stochastic dispersal in a heterogeneous landscape. Science 294, 813–817.
Kleczkowski, A., Grenfell, B., 1999. Mean-field-type equations for spread of epidemics: the 'small world' model. Phys. A 274, 355–360.
Kot, M., Lewis, M., van den, D.P., 1996. Dispersal data and the spread of invading organisms. Ecology 77, 2027–2042.
Kranz, J. ed., 2012. Epidemics of Plant Diseases: Mathematical Analysis and Modeling vol. 13. Springer Science & Business Media.
Kring, J.B., 1972. Flight behavior of aphids. Ann. Rev. Entomol. 17, 461–492.
Levin, S., Muller-Landau, H.C., Nathan, R., Chave, J., 2003. The ecology and evolution of seed dispersal: a theoretical perspective. Annu. Rev. Ecol. Evol. Syst. 34, 575–604.
Mollison, D., 1977. Spatial contact models for ecological and epidemic spread. J. R. Stat. Soc. B 34, 283–326.
Moslonka-Lefebvre, M., Finley, A., Dorigatti, I., Dehnen-Schmutz, K., Harwood, T., Jeger, M., Xu, X., Holdenrieder, O., Pautasso, M., 2011. Networks in plant epidemiology: from genes to landscapes, countries, and continents. Phytopathology 101, 392–403.
Mundt, C., Brophy, L., 1988. Influence of number of host genotype units on the effectiveness of host mixtures for disease control: a modeling approach. Phytopathology 78, 1087–1094.
Mundt, C., Brophy, L., Kolar, S., 1996. Effect of genotype unit number and spatial arrangement on severity of yellow rust in wheat cultivar mixtures. Plant Pathol. 45, 215–222.
Nathan, R., 2006. Long-distance dispersal of plants. Science 313, 786–788.
Nathan, R., Klein, E.K., Robledo-Arnuncio, J.J., Revilla, E., 2012. Dispersal kernels. In: Clobert, J., et al. (Eds.), Dispersal Ecology and Evolution. Oxford University Press, pp. 187–210.
Nault, L.R., 1997. Arthropod transmission of plant viruses: a new synthesis. Ann. Entomol. Soc. Am. 90, 521–541.
Paysour, R., Fry, W., 1982. Interplot interference: A model for planning field experiments with aerially disseminated pathogens. Cornell University Doctoral dissertation.
Penrose, M., 2003. Random Geometric Graphs. Oxford University Press.
Powell, G., Tosh, C.R., Hardie, J., 2006. Host plant selection by aphids: behavioral, evolutionary, and applied perspectives. Annu. Rev. Entomol. 51, 309–330.
Riley, S., Eames, K., Isham, V., Mollison, D., Trapman, P., 2015. Five challenges for spatial epidemic models. Epidemics 10, 68–71.
Rizzo, D., Garbelotto, M., Davidson, J., Slaughter, G.W., Koike, S., 2002. Phytophthora ramorum as the cause of extensive mortality of quercus spp. and lithocarpus densiflorus in california. Plant Dis. 86, 205–214.
Scherm, H., 1996. On the velocity of epidemic waves in model plant disease epidemics. Ecol. Modell. 87, 217–222.
Segarra, J., Jeger, M., Van den Bosch, F., 2001. Epidemic dynamics and patterns of plant diseases. Phytopathology 91, 1001–1010.
Shaw, M., 1995. Simulation of population expansion and spatial pattern when individual dispersal distributions do not decline exponentially with distance. Proc. R. Soc. Lond. B 259, 243–248.
Stacey, A., Truscott, J., Asher, M., Gilligan, C., 2004. A model for the invasion and spread of rhizomania in the united kingdom: implications for disease control strategies. Phytopathology 94, 209–215.
Swinton, J., Gilligan, C., 1996. Dutch elm disease and the future of the elm in the UK: a quantitative analysis. Proc. Trans. R. Soc. B 351, 605–615.
Vallaeys, V., Tyson, R., Lane, W., Deleersnijder, E., Hanert, E., 2017. A Lévy-flight diffusion model to predict transgenic pollen dispersal. J. R. Soc. Interface 14, 20160889.
Van den Bosch, F., Zadoks, J., Metz, J., 1988. Focus expansion in plant disease. II: realistic parameter-sparse models. Phytopathology 78, 59–64.
Van Maanen, A., Xu, X., 2003. Modelling plant disease epidemics. Eur. J. Plant Pathol. 109, 669–682.
Van Mieghem, P., Omic, J., Kooij, R., 2009. Virus spread in networks. IEEE/ACM Trans. Netw. 17, 1–14.
Waggoner, P., 1962. Weather, space, time, and chance of infection. Phytopathology 52, 1100–1108.
Xu, X., Ridout, M., 2000. Effects of quadrat size and shape, initial epidemic conditions, and spore dispersal gradient on spatial statistics of plant disease epidemics. Phytopathology 90, 738–750.